CHEMISTRY OF MATERIALS
Article

Chem. Mater. **2010,** *22,* 2395–2402 2395
DOI:10.1021/cm903844t

Seed Displacement, Epitaxial Synthesis of Rh/Pt Bimetallic Ultrathin Nanowires for Highly Selective Oxidizing Ethanol to CO_2

Qiang Yuan,[†,‡] Zhiyou Zhou,*[,§] Jing Zhuang,[†] and Xun Wang*[,†]

[†]*Department of Chemistry, Tsinghua University, Beijing 100084, P. R. China,* [‡]*Department of Chemistry, Guizhou University, Guiyang, Guizhou province 550025, P. R. China, and* [§]*Department of Chemistry, College of Chemistry and Chemical Engineering, Xiamen University, Xiamen 361005, P. R. China*

Received December 24, 2009. Revised Manuscript Received February 6, 2010

For the first time, the high-yield, branched Rh/Pt bimetallic ultrathin nanowires with nodes and stems have been synthesized by seed displacement, epitaxial growth method in aqueous solution containing Rh nanocubes seeds, K_2PtCl_6, and poly(vinyl pyrrolidone) (PVP). The quantities of Rh nanocubes play a key role in the formation of high-yield ultrathin nanowires. The results of EDS line scanning and elemental analysis map have shown that the Rh atoms distribute discretely in the wires. The electrocatalytic properties of the Rh/Pt bimetal alloys, Rh nanocubes, and commercial Pt black toward ethanol oxidation have been investigated. The Rh/Pt ultrathin nanowires have displayed enhanced electrocatalytic performance and selectivity. The results of in situ FTIR have shown that the selectivity to the complete oxidation of ethanol to CO_2 of Rh/Pt bimetallic ultrathin nanowires is at least 2.69 times higher as compared with the commercial Pt black.

Introduction

Nanowires have been widely used in many important fields such as optics, magnetics, catalysis, environmental remediation, and biosensor for many years.[1−7] To date, many synthetic methods, including templating,[8−14] ligand control,[15−21] and oriented attachment,[22−26] have been exploited to synthesize ingornic nanowires. Among these, solution-based method has been used to synthesize nanowire with diameter sub-5 nm. For example, single-component noble metal Au, Ag, Pt, and Pd nanowires have been achieved by an oleylamine(OA) system, polyol process and phase transfer method.[27−33] Nevertheless,

*Corresponding author. E-mail: wangxun@mail.tsinghua.edu.cn (X.W.); zhouzy@xmu.edu.cn (Z.Z.).

(1) Cui, Y.; Wei, Q. Q.; Park, H. K.; Lieber, C. M. *Science* **2001**, *293*, 1289–1292.
(2) Nhut, J. M.; Pesant, L.; Wine, J. P. G.; Guille, J.; Pham-Huu, C.; Ledoux, M. J. *Appl. Catal., A* **2003**, *254*, 345–363.
(3) Yavuz, C. T.; Mayo, J. T.; Yu, W. W.; Prakash, A.; Falkner, J. C.; Yean, S.; Cong, L. L.; Shipley, H. J.; Kan, A.; Tomson, M.; Natelson, D.; Colvin, V. L. *Science* **2006**, *314*, 964–967.
(4) Yuan, J.; Liu, X.; Akbulut, O.; Hu, J.; Suib, S. L.; Kong, J.; Stellacci, F. Nat. *Nanotechnology* **2008**, *3*, 332–336.
(5) Nakayama, Y.; Pauzauskie1, P. J.; Radenovic, A.; Onorato1, R. M.; Saykally1, R. J.; Liphardt, J.; Yang, P. D. *Nature* **2007**, *447*, 1098–1102.
(6) Stern, E.; Klemic, J. F.; Routenberg, D. A.; Wyrembak, P. N.; Turner-Evans, D. B.; Hamilton, A. D.; LaVan, D. A.; Fahmy, T. M.; Reed, M. A. *Nature* **2007**, *445*, 519–522.
(7) Thurn-Albrecht, T.; Schotter, J.; Ka-stle, G. A.; Emley, N.; Shibauchi, T.; Krusin-Elbaum, L.; Guarini, K.; Black, C. T.; Tuominen, M. T.; Russell1, T. P. *Science* **2000**, *290*, 2126–2129.
(8) Coleman, N. R. B.; Morris, M. A.; Spalding, T. R.; Holmes, J. D. *J. Am. Chem. Soc.* **2001**, *123*, 187–188.
(9) Crowley, T. A.; Ziegler, K. J.; Lyons, D. M.; Erts, D.; Olin, H.; Holmes, M. A. J. D. *Chem. Mater.* **2003**, *15*, 3518–3522.
(10) Ziegler, K. J.; Polyakov, B.; Kulkarni, J. S.; Crowley, T. A.; Ryan, K. M.; Morris, M. A.; Erts, D.; Holmes, J. D. *J. Mater. Chem.* **2004**, *14*, 585–589.
(11) Wu, Y.; Cui, Y.; Huynh, L.; Barrelet, C. J.; Bell, D. C.; Lieber, C. M. *Nano Lett.* **2004**, *4*, 433–436.
(12) Holmes, J. D.; Johnston, K. P.; Doty, R. C.; Korgel, B. A. *Science* **2000**, *287*, 1471–1473.
(13) Grebinski, J. W.; Hull, K. L.; Zhang, J.; Kosel, T. H.; Kuno, M. *Chem. Mater.* **2004**, *16*, 5260–5272.
(14) Kuno, M.; Ahmad, O.; Protasenko, V.; Bacinello, D.; Kosel, T. H. *Chem. Mater.* **2006**, *18*, 5722–5732.
(15) Peng, X. G.; Manna, L.; Yang, W. D.; Wickham, J.; Scher, E.; Kadavanich, A.; Alivisatos, A. P. *Nature* **2000**, *404*, 59–61.
(16) Peng, X. *Adv. Mater.* **2003**, *15*, 459–463.
(17) Liu, Z. P.; Xu, D.; Liang, J. B.; Shen, J. M.; Zhang, S. Y.; Qian, Y. T. *J. Phys. Chem. B* **2005**, *109*, 10699–10704.
(18) Cademartiri, L.; Malakooti, R.; O'Brien, P. G.; Migliori, A.; Petrov, S.; Kherani, N. P.; Ozin, G. A. *Angew. Chem., Int. Ed.* **2008**, *47*, 3814–3817.
(19) Malakooti, R.; Cademartiri, L.; Migliori, A.; Ozin, G. A. *J. Mater. Chem.* **2008**, *18*, 66–69.
(20) Park, K. H.; Choi, J.; Kim, H. J.; Lee, J. B.; Son, S. U. *Chem. Mater.* **2007**, *19*, 3861–3863.
(21) Cademartiri, L.; Bertolotti, J.; Sapienza, R.; Wiersma, D. S.; Kitaev, V.; Ozin, G. A. *J. Phys. Chem. B* **2006**, *110*, 671–673.
(22) Banfield, J. F.; Welch, S. A.; Zhang, H. Z.; Ebert, T. T.; Penn, R. L. *Science* **2000**, *289*, 751–754.
(23) Penn, R. L.; Banfield, J. F. *Science* **1998**, *281*, 969–971.
(24) Colfen, H.; Antonietti, M. *Angew. Chem., Int. Ed.* **2005**, *44*, 5576–5591.
(25) Pradhan, N.; Xu, H. F.; Peng, X. G. *Nano Lett.* **2006**, *6*, 720–724.
(26) Cho, K.-S.; Talapin, D. V.; Gaschler, W.; Murray, C. B. *J. Am. Chem. Soc.* **2005**, *127*, 7140–7147.
(27) Lu, X.; Yavuz, M. S.; Tuan, H.-Y.; Korgel, B. A.; Xia, Y. *J. Am. Chem. Soc.* **2008**, *130*, 8900–8901.
(28) Wang, C.; Hu, Y.; Lieber, C. M.; Sun, S. *J. Am. Chem. Soc.* **2008**, *130*, 8902–8903.
(29) Huo, Z.; Tsung, C.-K.; Huang, W.; Zhang, X.; Yang, P. *Nano Lett.* **2008**, *8*, 2041–2044.
(30) Chen, J.; Herricks, T.; Geissler, M.; Xia, Y. *J. Am. Chem. Soc.* **2004**, *126*, 10854–10855.
(31) Song, Y.; Garcia, R. M.; Dorin, Rachel M.; Wang, H.; Qiu, Y.; Coker, E. N.; Steen, W. A.; Miller, J. E.; Shelnutt, J. A. *Nano Lett.* **2007**, *7*, 3650–3655.
(32) Teng, X.; Han, W.-Q.; Ku, W.; Hücker, M. *Angew. Chem., Int. Ed.* **2008**, *47*, 2055–2058.
(33) Sun, Y.; Gates, B.; Mayers, B.; Xia, Y. *Nano Lett.* **2002**, *2*, 165–168.

Published on Web 02/18/2010

noble bimetallic nanowires have a limited successful examples.[34,35] Therefore, the synthesis of bimetal nanowires still remains changeable. Seed-mediated epitaxial growth method for controlling the morphology and composition of bimetallic nanostructures is often exploited to synthesize binary metallic alloys in solution-phase methods.[36,37] Our previous result[35] has shown that sub-4 nm Pd/Pt bimetallic ultrathin nanowires with length up to 300 nm can be achieved by a seed-mediated method. It greatly encouraged us to design a new class of Rh/Pt bimetal nanowires for enthanol electrocatalytic application.

Ethanol is a promising fuel in low-temperature fuel cells application because of not only its abundant feedstock from agricultural products and the fermentation of biomass but also higher energy density and lower toxicity compared with its counterparts such as methanol and formic acid. Platinum is commonly used as catalyst in direct ethanol fuel cells (DEFC). Previous studies[38−40] indicated that ethanol oxidation mainly concerns sequential and parallel reactions as following: $CH_3CH_2OH \rightarrow [CH_3CH_2OH]_{ad} \rightarrow C1_{ad}$, $C2_{ad} \rightarrow CO_2$ (total oxidation) (1); $CH_3CH_2OH \rightarrow [CH_3CH_2OH]_{ad} \rightarrow CH_3CHO \rightarrow CH_3COOH$ (partial oxidation) (2). Unfortunately, in situ infrared reflection−absorption spectrometry (IRRAS) and differential electrochemical mass spectroscopy[41−45] have shown that the reaction 2 is predominant, namely acetic acid is the main "end-product"; CO_2 has the lowest selectivity among the three products,[46,47] which tremendously lowered the efficiency of energy utilization and impeded the use of ethanol in DEFC. Therefore, the rational design of catalysts for highly selective oxidizing ethanol to CO_2 still remains challenging.

The breaking of strong C−C bond of ethanol is a key factor for deeply oxidizing ethanol to CO_2. During the past decade, a number of efforts have been made for enhancing the CO_2 selectivity. Many Pt-based alloys such as Pt/Ru, Pt/Rh, Pt/Sn and Pt/Rh/Sn have been widely investigated.[48−55] The results have showed the alloy boosted up the ethanol oxidation owing to their unique surface structure and electron interaction. However, the limited successes were achieved for highly selective oxidizing ethanol to CO_2. Meanwhile, the studies have shown the Rhodium has a special effect on cleavage of C−C bond.[53,56,57] Therefore, the synthesis of monodispersed, well-defined morphology and size-controlled Rh/Pt bimetallic alloys and investigating their dependence between electrocatalytic performance and structures on ethanol oxidation are of significance.

Experimental Section

Chemicals. PVP (CP, MW = 30000), NaBr (A.R.) and sodium lauryl sulfate (SLS) (A.R.) ethanol (99.99%) were purchased from Beijing Chemical Reagent Company. $RhCl_3 \cdot nH_2O$ (A.R., Rh content: 40 wt %), $PdCl_2$ (A.R.), and K_2PtCl_6 (A.R.) were purchased form Beijing research institute for nonferrous metals. $HClO_4$ were purchased from Alfa Aesar. Pt black was purchased from Johnson Matthey. Chemicals were used as received without further purification. Deionized water was used for the synthesis of nanocrystals.

Synthesis of Rh Nanocubes Crystal. Seven milliliters of H_2O, 1.0 mL of $RhCl_3$ aqueous solution (0.1 M), 103 mg of NaBr, 300 mg of PVP (MW = 30 000), and 289 mg of SLS were added to a beaker and stirred for 5 min. The resulting homogeneous brown solution was transferred to a 12 mL Teflon-lined stainless-steel autoclave. The sealed vessel was then heated at 220 °C for 12 h before it was cooled to room temperature. The products were separated via centrifugation for several times by deionized water. The products were then dispersed with deionized water.

Synthesis of Rh/Pt Bimetal Nanowires. Desired quantity of Rh cubes (0.233 mg/mL Rh cubes, calculated from ICP-OES; i.e., 0.25, 0.50, and 1.0 mL) aqueous solution, 100 mg of PVP (MW = 30 000) and 24.0 mg of K_2PtCl_6 were added into water and stirred for 5 min (total volume: 7.5 mL). The resulting homogeneous solution was transferred to a 12 mL Teflon-lined stainless-steel autoclave. The sealed vessel was then heated at 200 °C for a desired time (i.e., 6 and 12 h) before it was cooled to room temperature. The products were separated via centrifugation for several times by deionized water. Then the products were dispersed with ethanol.

Instruments. The size and morphology of the nanocrystals were determined by a Tecnai G2 F20 S-Twin high-resolution transmission electron microscope (HRTEM) at 200 kV. The STEM, element analysis mapping and EDS line scanning were determined by a Titan 80−300 Cs-corrected TEM with resolution 0.08 nm at 300 kV. The ICP-OES of samples were performed on IRIS Intrepid II XSP (ThermoFisher). Working

(34) Teng, X.; Feygenson, M.; Wang, Q.; He, J.; Du, W.; Frenkel, A. I.; Han, W.; Aronson, M. *Nano Lett*. **2009**, *9*, 3177–3184.
(35) Yuan, Q.; Zhuang, J.; Wang, X. *Chem. Commun*. **2009**, *43*, 6613–6615.
(36) Fan, F. R.; Liu, D. Y.; Wu, Y.; Duan, S.; Xie, Z. X.; Jiang, Z. Y.; Tian, Z. Q. *J. Am. Chem. Soc*. **2008**, *130*, 6949–6591.
(37) Habas, S. E.; Lee, H.; Radmilovic, V.; Somorjai, G. A.; Yang, P. D. *Nat. Mater*. **2007**, *6*, 692–697.
(38) Colmati, F.; Tremiliosi-Filho, G.; Gonzalez, E. R.; Berná, A.; Herrero, E.; Feliu, J. M. *Faraday Discuss*. **2009**, *140*, 379–397.
(39) Vigier, F.; Rousseau, S.; Coutanceau, C.; Leger, J. M.; Lamy, C. *Top. Catal*. **2006**, *40*, 111–121.
(40) Camara, G. A.; Iwasita, T. *J. Electroanal. Chem*. **2005**, *578*, 315–321.
(41) Willsau, J.; Heitbaum, J. *J. Electroanal. Chem*. **1985**, *194*, 27–35.
(42) Iwasita, T.; Pastor, E. *Electrochim. Acta* **1994**, *39*, 531–537.
(43) Hitmi, H.; Belgsir, E. M.; Leger, J.-M.; Lamy, C.; Lezna, R. O. *Electrochim. Acta* **1994**, *39*, 407–415.
(44) Gootzen, J. F. E.; Visscher, W.; Van Veen, J. A. R. *Langmuir* **1996**, *12*, 5076–5082.
(45) Schmidt, V. M.; Ianniello, R.; Pastor, E.; Gonzalez, S. *J. Phys. Chem*. **1996**, *100*, 17901–17908.
(46) Xia, X. H.; Liess, H.−D.; Iwasita, T. *J. Electroanal. Chem*. **1997**, *437*, 233–240.
(47) Wang, H.-F.; Liu, Z.-P. *J. Am. Chem. Soc*. **2008**, *130*, 10996–11004.
(48) Lamy, C.; Rousseau, S.; Belgsir, E. M.; Coutanceau, C.; Leger, J.-M. *Electrochim. Acta* **2004**, *49*, 3901–3908.
(49) Antolini, E. *J. Power Sources* **2007**, *170*, 1–12.
(50) Mann, J.; Yao, N.; Bocarsly, A. B. *Langmuir* **2006**, *22*, 10432–10436.
(51) Kowal, A.; Li; Shao, M.; M.; Sasaki, K.; Vukmirovic, M. B.; Zhang, J.; Marinkovic, N. S.; Liu, P.; Frenkel, A. I.; Adzic, R. R. *Nat. Mater*. **2009**, *8*, 325–330.
(52) Fujiwara, N.; Friedrich, K. A.; Stimming, U. *J. Electroanal. Chem*. **1999**, *472*, 120–125.
(53) Lima, F. H. B.; Gonzalez, E. R. *Electrochim. Acta* **2008**, *53*, 2963–2971.
(54) Bergamaski, K.; Gonzalez, E. R.; Nart, F. C. *Electrochim. Acta* **2008**, *53*, 4396–4406.
(55) de Souza, J. P. I.; Queiroz, S. L.; Bergamaski, K.; Gonzalez, E. R.; Nart, F. C. *J. Phys. Chem. B* **2002**, *106*, 9825–9830.
(56) Méndez, E.; Rodríguez, J. L.; Arévalo, M. C.; Pastor, E. *Langmuir* **2002**, *18*, 763–772.
(57) Sheng, P.-Y.; Yee, A.; Bowmaker, G. A.; Idriss, H. *J. Catal*. **2002**, *208*, 393–403.

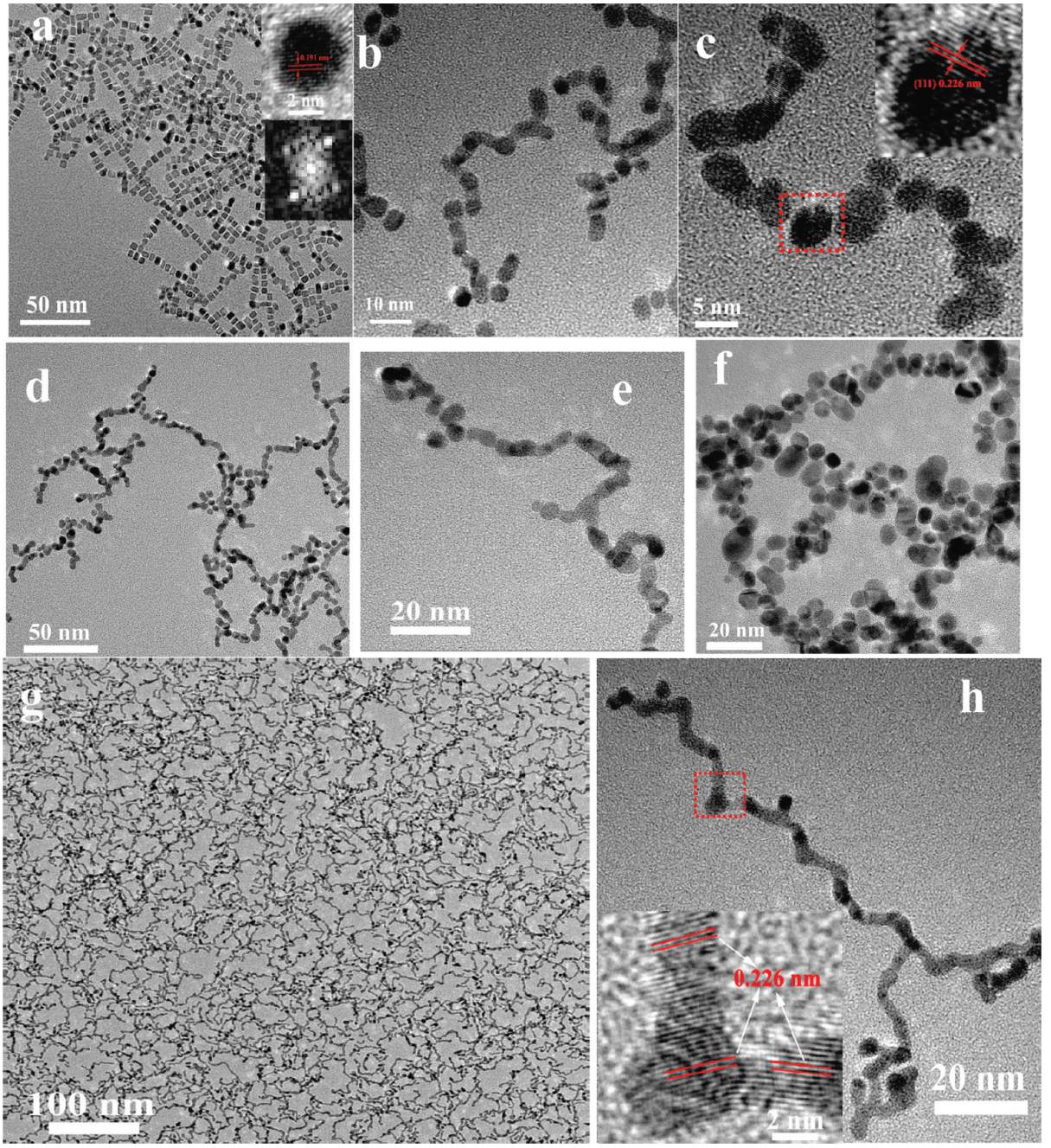

Figure 1. (a) TEM images of Rh nanocube crystals (inset, HRTEM image and FT patterns of single nanocube), and Rh/Pt heterostructures. (b, c) Rh/Pt 1, 0.5 mL Rh cube seeds, time 6 h; and (d, e) Rh/Pt 2, 0.5 mL Rh cube seeds, time 12 h; (f) 1.0 mL Rh cube seeds, time 12 h; (g, h) Rh/Pt 3, 0.25 mL Rh cube seeds, reaction time 12 h.

parameters: RF Power: 1150 W, Nebulizer Flow: 26.0 PSI, Auxiliary gas: 1.0 LPM.

Test of Electrocatalytic Activity. Electrochemical experiments were carried out in a standard three-electrode cell at room temperature (about 25 °C) controlled by PAR 263A potentiostat/galvanostat (EG&G). The super pure water (18 MΩ cm) purified through a Milli-Q Lab system (Nihon Millipore Ltd.) was used as solvent.

The super pure water dispersion of purified nanoparticles was deposited on a glassy carbon electrode (GC, ϕ5 mm; Takai Carbon Co., Ltd., Tokyo, Japan) to get the working electrodes after evaporation of solvent under an IR lamp. A reversible hydrogen electrode (RHE) and a platinum foil were used as the reference and counter electrode, respectively.

The cyclic voltammograms (CVs) were obtained in nitrogen-saturated $HClO_4$ (0.1 M) solution, and the potential was scanned from 0.05 to 1.4 V (RHE) at a scan rate 20 mV/s. Voltammogram measurment for ethanol oxidation was carried out in ethanol (0.1 M) + $HClO_4$ (0.1 M) solution, and the potential was scanned from 0.05 to 1.4 V (RHE) at a scan rate 20 mV/s.

In situ Fourier Transform Infrared Spectra. In situ FTIR studies were carried out with a Nicolet Nexus 870 Fourier-transform infrared spectrometer equipped with a mercury cadmium telluride detector cooled with liquid nitrogen. An unpolarized light beam was used. The spectral resolution was set to 8 cm^{-1} and 1200 interferograms were together added to each spectrum. The reference spectrum was collected at 0.05 V in the

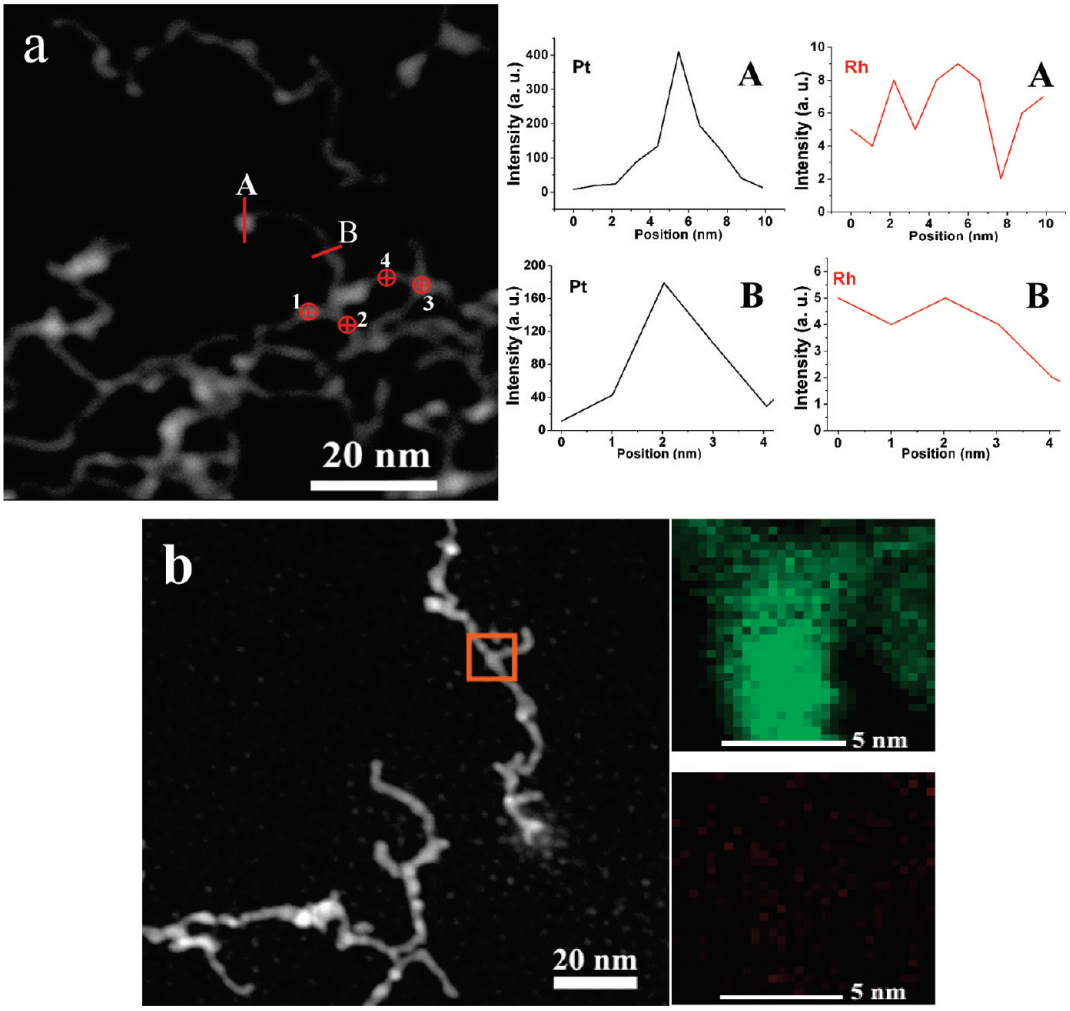

Figure 2. High-angle annular dark field (HAADF)-STEM images of Rh/Pt 3 ultrathin nanowires. (a) and (A, B) cross-sectional compositional EDS line scanning profiles and EDS positions (1−4, corresponding EDS profiles are shown in Figure S5 in the Supporting Information); (b) selected-region (the golden rectangle) element analysis maps of Pt (green) and Rh (golden).

same solution with ethanol (0.1 M) and $HClO_4$ (0.1 M). A CaF_2 planar was used as the infrared window.

Results and Discussions

Rh/Pt Bimetal Nanowires Formation. The Rh/Pt nanowires were synthesized using a sequential aqueous-phase route. First, we synthesized uniform, narrow-size distribution Rh nanocubes with an average size of 3.3 ± 0.2 nm by reducing $RhCl_3$ in the presence of PVP and Br anion through a one-pot method.[35] The synthesized Rh nanocubes and K_2PtCl_6 were then used as seeds and precursor, respectively, for producing Rh/Pt nanowires only extra addition a small quantity of PVP. Figure 1a and Figure S1 show transmission electron microscopy (TEM) images of the as-synthesized Rh nanocubes. The nanocubes were highly dispersed and nearly 95% in cubes shape and had an average size of 3.3 ± 0.2 nm. A high-resolution TEM (HRTEM) image of a single Rh nanocube and the corresponding Fourier-transform (FT) (Figure 1a inset) pattern indicate that it was a single crystal with its surface being enclosed by {100} facets and the interval between two lattice fringes was examined to be 0.191 nm, in accord with the (200) lattice spacing of the fcc Rhodium.

The as-obtained Rh nanocubes were utilized as seeds for the controlled growth of Rh/Pt bimetal nanowires. Figure 1b and Figure S2 show the TEM images of the as-synthesized Rh/Pt bimetal alloys after a reaction time of 6 h with the quantity of 0.5 mL Rh seeds (Marked Rh/Pt 1). The product consists of elongated particles with an average diameter of 5.0 ± 0.3 nm and bent short rods with the length of 10−30 nm. The surface lattice fringe intervals of the elongated particle is 0.226 nm (Figure 1c, inset), which is corresponding to the (111) facet of fcc Platinum. And the particles and bent rods have obvious contrast of bright and dark. Furthermore, a typical intermediate of bent rods was captured by TEM (Figure 1c), it shows a strong orientation growth tendency to 1D structure through linkage with abutting ends of particles and/or rods (see Figure S2 in the Supporting Information). This is perhaps one of the reasons why there has a heavy dark at the junctions of the rods. With the reaction time increasing to 12 h, the particles evidently decreased, whereas the dominant wires appeared with length reaching about 60 nm (marked Rh/Pt 2, Figure 1d, e and Figure S3 in the Supporting Information). It is of interest that the product is only made of particles with the

quantity of Rh seeds increasing to 1.0 mL. The size of particles is not well-distributed and average diameter is beyond 7.0 nm (Figure1f). However, when the quantity of Rh seeds is decreased to 0.25 mL, the product was made of nearly 100% nanowires with nearly 100% yield (marked Rh/Pt 3, Figure 1g and Figure S4 in the Supporting Information). The nanowires are made of nodes (the heavy dark dots) and smaller stems with average diameter below 4.3 and 3.2 nm, respectively. The length of such ultrathin nanowires can be up to more than 300 nm (Figure 1h and Figure S4 in the Supporting Information). The lattice fringe of nanowire surface with intervals of 0.226 is clearly observed (Figure 2f, inset), ascribed to (111) of fcc platinum. To indentify the components of nodes and stems of bimetal nanowires, we combined element analysis mapping with EDS line scanning and STEM-EDS to analyze the compositions of representative positions on aberration-corrected HRTEM (FEI Titan 80−300). The STEM image, EDS line scanning profiles and EDS profiles taken from the different positions of wires are shown in Figure 2a and Figure S5 in the Supporting Information. The results displayed that the wires are nearly made of Pt atoms, whereas the signals of Rh were very weak and hard to be detected. Maybe this was caused by the extremely few quantities of Rh atoms relative to Pt atoms. This suggestion is supported by the results of ICP-OES (see Table S1 in the Supporting Information). The quantities of Rh is only 1.08 at % in the wires, which is consistent with the theoretic ratio value of Rh atoms. To further distinguish the distribution of Pt and Rh in the wires, we used the technology of element analysis map. Figure 2b shows the STEM image and selected-area element analysis maps of Pt and Rh, displaying that Pt atoms distribute in the whole area (green), whereas, the Rh atoms just distribute discretely with few quantities of dots (golden). The above evidence indicates that the Rh seeds cube was displaced by Pt, whereas the Rh were rereduced and distributed the wires discretely.

Lattice mismatch plays a critically important role in the growth of the secondary metal on seeds, which determined the growth mode through either conformal or anisotropic growth and decided the final shape of product.[36,37] The lattice mismatch of Rh/Pt is about 3.2%. Yang and co-workers have reported that high lattice mismatch effectively prevents conformal overgrowth of Au on the Pt nanocubes (4.08% mismatch for Au/Pt). However, our previous result [35] showed that low lattice mismatch of Pd/Pt (0.77% mismatch) can also form heterostructured ultrathin nanowires by using Pd nanocubes as seeds. Therefore, in our system, the lattice mismatch for formation of nanowires is not a key factor. Maybe, the Pt displacing Rh to produce Pt seeds is a key process. On the other hand, the formation of Rh/Pt wires was also controlled by the reduction rate of Pt by an autocatalytic process, which has been used to explain the

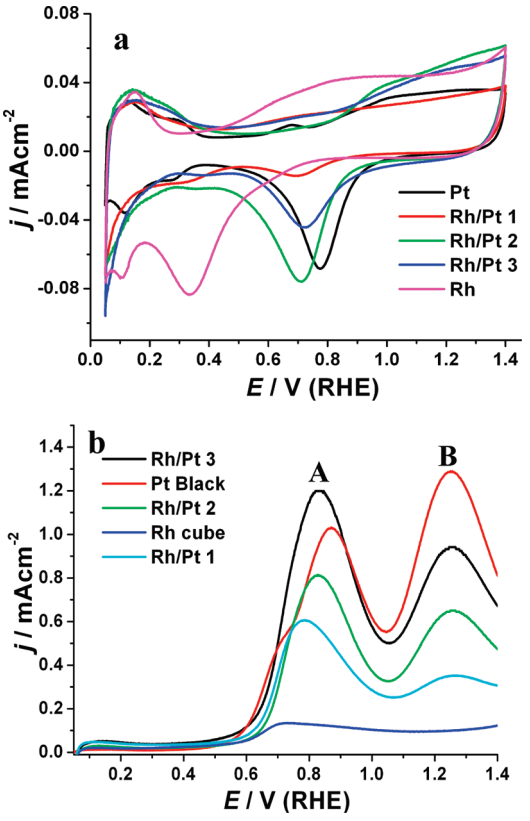

Figure 3. Cyclic voltammetric curves (CVs) of Rh cubes, commercial Pt black, and Rh/Pt bimetal alloys in (a) a 0.1 M $HClO_4$ solution and (b) a 0.1 M ethanol + 0.1 M $HClO_4$ solution.

formation of branched nanostructures of Pt.[58−61] This suggestion is also supported by the EDS line scanning, element analysis maps, and the quantity of Rh seeds. The above-mentioned results show that the more the seeds were, the faster the Pt^{4+} were reduced, and the more difficult it was for the wires to form because of the faster reduction and growth of Pt to form individually large particles. On the basis of these results, we deduced that the formation mechanism of heterostructured Rh/Pt ultrathin wires processed as following: The first step was that the Pt^{4+} ions diffused the surface of Rh cubes and reducd by surface Rh seeds via galvanic replacement, at the same time, the Pt nucleated and grew along the lowest energy facet orientation (111) to form Pt particles. Then the rest of Pt ions and reoxidized Rh ions were reduced by autocatalytic process and anisotropically grew along the (111) facets of the Pt shell to form the short rods. Finally, the rods grew into wires by oriented attachment at the ends of each short rods. The growth mode led to the formation of wire structures with heavy nodes and stems. The intermediates of particles, elongated particles and short rods provided evidence for the formation mechanism. In the present system, the Rh seeds probably served as media for providing a well-defined surface for the

(58) Song, Y.; Yang, Y.; Medforth, C. J.; Pereira, E.; Singh, A. K.; Xu, H.; Jiang, Y.; Brinker, C. J.; Swol, F. v.; Shelnutt, J. A. *J. Am. Chem. Soc.* **2004**, *126*, 635–645.
(59) Chen, J.; Herricks, T.; Xia, Y. N. *Angew. Chem., Int. Ed.* **2005**, *44*, 2589–2592.
(60) Teng, X.; Liang, X.; Maksimuk, S.; Yang, H. *Small* **2006**, *2*, 249–253.
(61) Lim, B.; Jiang, M.; Camargo, P. H. C.; Cho, E. C.; Tao, J.; Lu, X.; Zhu, Y.; Xia, Y. N. *Science* **2009**, *324*, 1302–1305.

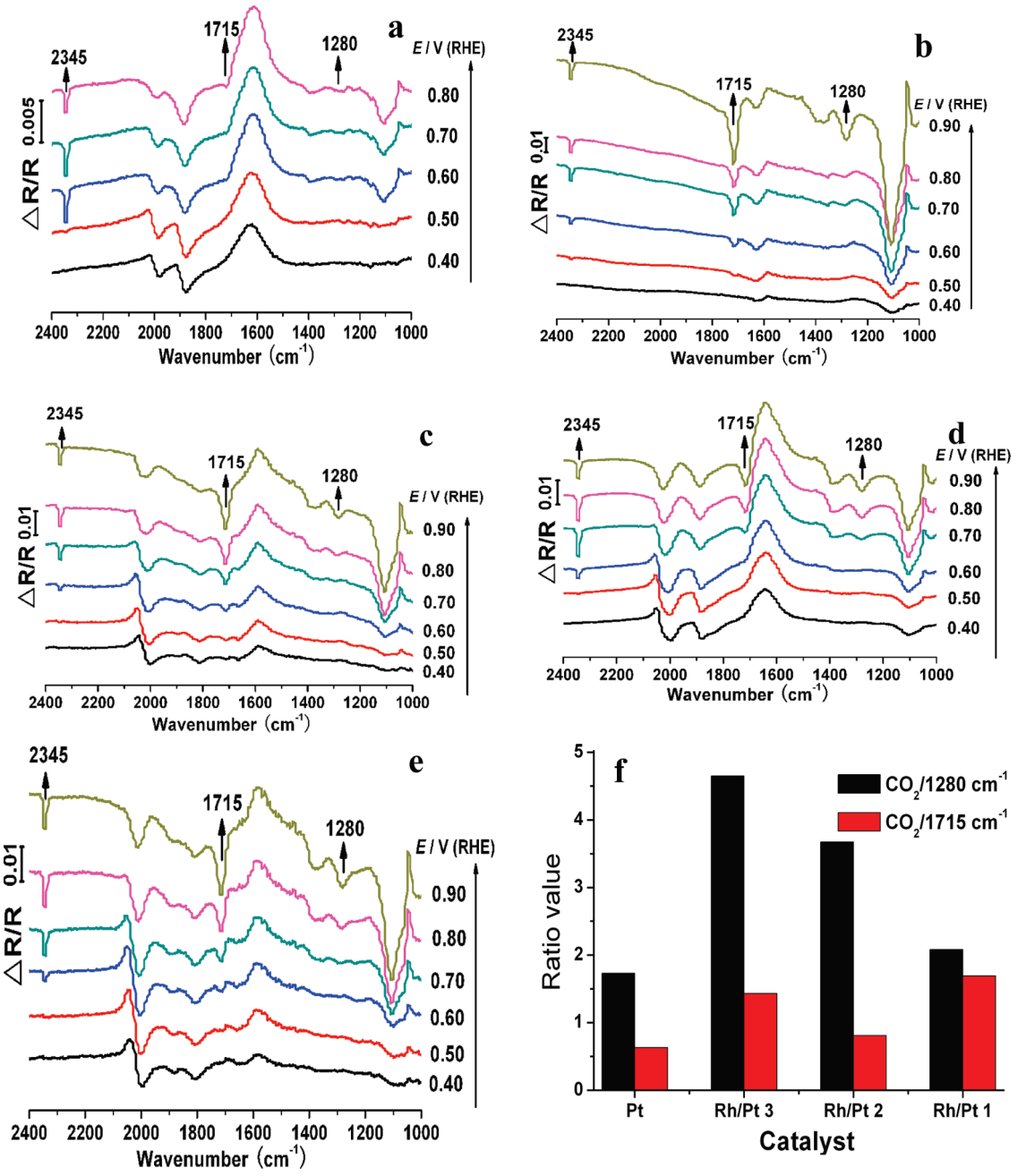

Figure 4. In situ FTIR spectra of samples for ethanol oxidation in in a 0.1 M ethanol + 0.1 M $HClO_4$ solution. (a) Rh cubes. (b) Commercial Pt black. (c) Rh/Pt 1. (d) Rh/Pt 2. (e) Rh/Pt 3. (f) Band intensity comparisons of CO_2 with 1280 and 1715 cm^{-1} of commercial Pt black and Rh/Pt heterostructures at 0.8 V.

growth of Pt, which is in favor of reduction, nucleation and growth of Pt precursor. For supporting this point, we did the comparable experiment at the same conditions of the synthesis of Rh/Pt wires in the absence of Rh cubes seeds. The result was that we did not get any related product of single Pt, which showed it was difficult to nucleate and grow for Pt without Rh seeds in present synthetic conditions and also indirectly proved the above suggestion. Moreover, the PVP maybe played roles as stabilizing agent and reducing agent in the present synthesis system. Because there also had no product in the absence of PVP.

Electrocatalytic Test toward Ethanol. The catalytic activity of Rh/Pt bimetal alloy toward ethanol oxidation was tested against single Rh cubes and commercial Pt black. The electrodes were immersed in nitrogen-saturated $HClO_4$ (0.1 M) solution, and the potential was scanned from 0.05 to 1.4 V (vs reversible hydrogen electrode, RHE) at a scan rate 20 mV/s to obtain the cyclic voltammograms (CVs) (Figure 3a). The hydrogen desorption electric charges calculated from CVs were used to estimate the electrochemically active surface area (ECSA) of catalysts. The centers of oxygen desorption potential peak of commercial Pt black and Rh cubes locate at 0.77 and 0.33 V, respectively. However, the centers of oxygen desorption peak of Rh/Pt alloys are between that of Rh and commercial Pt black, and the shapes of CVs obviously differ from that of commercial

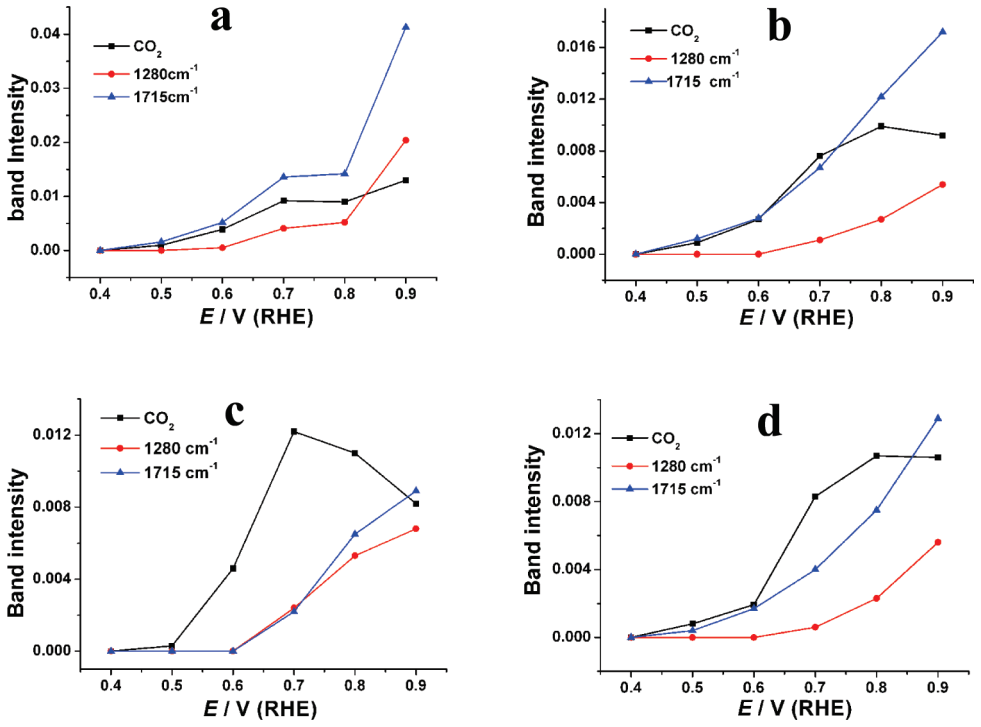

Figure 5. Band intensities as a function of potential associated with CO_2, 1715 and 1280 cm^{-1} of ethanol oxidation on (a) commercial Pt Black, (b) Rh/Pt 1, (c) Rh/Pt 2, and (d) Rh/Pt 3 ultrathin wires surfaces. Note: black squares, 2345 cm^{-1} band of CO_2; blue triangles, 1715 cm^{-1} C=O stretch vibration in acetaldehyde and/or acetic acid; red circles, 1280 cm^{-1} band of acetic acid.

Pt black and Rh cubes. For example, the oxygen desorption peaks of ultrathin nanowires RhPt 3 locate at 0.72 and 0.40 V, respectively. It indicates strong electron interaction between Rh and Pt atoms among this sample.

The electrocatalytic activities of catalysts were investigated in the ethanol (0.1 M) + $HClO_4$ (0.1 M) solution at a scan rate of 20 mV/s from 0.05 to 1.4 V at room temperature (25 °C). The current density (j) was calculated by normalizing the oxidation current to ECSA, so that it directly corresponds to the catalytic activity of unit surface area (Pt, Rh, or Rh/Pt) of the sample. Thus, it can be directly compared for different samples. Figure 3b shows the comparison of electrocatalytic properties of the Rh/Pt bimetal alloys, Rh nanocubes and commercial Pt black. There are two oxidation peaks for ethanol oxidation over commercial Pt black and Rh/Pt alloys. While for Rh catalyst it has a weak and broad oxidation peak. The peak potential of commercial Pt black is 0.87 V (Peak A) and 1.25 V (Peak B), respectively. Commonly, Peak A is ascribed to oxidizing ethanol to acetaldehyde, acetic acid and CO_2, and Peak B is almost completely ascribed to acetic acid.[43,62] Furthermore, the peak intensity of Peak B is higher than that of Peak A. It means that the acetic acid is mainly "end-product" for pure Pt catalyst. It is of interest that the peak potential of Peak A decreased obviously with increasing of Rh content, however, this phenomenon did not happen for Peak B. At the same time, the intensity of Peak B that associated with acetic acid decreased substantially with increasing Rh content. Finally, it almost disappeared for pure Rh cubes. Besides, the peak current also decreased with the Rh content increase. The peak current is only 0.13 mA cm^{-2} on pure Rh cubes. For the sample of typical bimetallic ultrathin nanowires Rh/Pt 3, the peak currents are 1.20 (peak potential locates at 0.83 V) and 0.94 mA cm^{-2} (peak potential locates at 1.25 V), meanwhile, the corresponding values of the commercial Pt black are 1.03 and 1.29 mA cm^{-2}, respectively. It means that the introduction of Rh can enhance the activity of ethanol oxidation and lower the acetic acid product.

In situ FTIR Characterization for Ethanol Oxidation. In situ FTIR spectroscopic studies were commonly used to identify the intermediates and products of ethanol oxidation. Three sets of spectra for Rh cubes, commercial Pt black and typical Rh/Pt 3 ultrathin nanowires are shown in Figure 4a–c. The band at 2345 cm^{-1} is signature peak for the O=C=O asymmetric stretch vibration of CO_2, which reflects the cleavage of the C–C bond in ethanol oxidation. The band at ~1715 cm^{-1} is the stretching vibration of the C=O bond in acetic acid and/or acetaldehyde because of possible overlap at this location. A well-defined band at 1285 cm^{-1} is the characteristic absorption of C–O stretching in acetic acid, which is usually used for quantitative analysis of acetic acid. The upward band at 1047 cm^{-1} is the signature peak for the C–O stretching vibration of CH_3CH_2OH, representing the consumption of ethanol due to oxidation. For pure Rh cubes, the bands intensity of 1715 cm^{-1} is very weak and that of 1285 cm^{-1} do not appear essentially (Figure 4a). Namely, CO_2 was the only detected main product. This result is similar to that reported by Tacconi

(62) Chang, S.-C.; Leung, L.-W. H.; Weaver, M. J. *J. Phys. Chem.* **1990**, *94*, 6013–6021.

et al.[63] They observed that CO_2 was the main product on a smooth polycrystalline Rh electrode in 0.5 M $HClO_4$ + 0.1 M CH_3CH_2OH solution. While the two CO chemisorption bands appeared on Rh surface, located at around 1900 and 2000 cm^{-1} and ascribed to bridged and linear CO, respectively (Figure 4a). The two bands also appeared on Rh/Pt 3 bimetal nanowires (Figure 4e) and other Rh/Pt bimetal alloys (Figure 4c and 4d). These indicate that the Rh exists in the surface of Rh/Pt bimetal alloys. The band intensities of acetic acid and/or acetaldehyde is obviously stronger than that of CO_2 on commercial Pt black at the potential beyond 0.4 V (Figures 4b and 5a). The comparison of ratio of band intensity of CO_2 to acetic acid (located at 1285 and 1715 cm^{-1}) for in situ FTIR spectra of ethanol oxidation on the commercial Pt black and Rh/Pt heterostructures catalysts at 0.80 V was illustrated in Figure 4f. Obviously, much more CO_2 and much less acetic acid were formed on Rh/Pt alloys catalysts for ethanol oxidation as compared with commercial Pt black (Figure 5c,d). For example, the band intensities of CO_2 at 2345 cm^{-1} and acetic acid at 1285 cm^{-1} are 0.0107 and 0.0023, respectively, on the Rh/Pt 3 catalysts, and corresponding values are 0.0090 and 0.0052 on the commercial Pt black. The ratio of band intensities of CO_2 to acetic acid on the Rh/Pt 3 is 2.69 times to that on the commercial Pt black (i.e., 4.65 vs 1.73). Besides, the ratio of band intensities of CO_2 to that located at 1715 cm^{-1} on the Rh/Pt 3 is 2.27 times to that on the commercial Pt black (i.e., 1.43 vs 0.63). It implies that the introduction of Rh is favor of splitting the C−C bond and enhances the CO_2 selectivity. Among these samples, the ultrathin Rh/Pt 3 ultrathin nanowires showed the best activity and selectivity toward oxidizing ethanol to CO_2 (Figure 3b and Figure 4e) because their smallest dimension and consecutive structure are more in favor of transmitting electrons.[64] These results clearly demonstrated that the Rh/Pt ultrathin nanowires do have substantially enhanced the reactivity of breaking C−C bond in ethanol, and as a consequence displayed a much higher selectivity to the complete oxidation of ethanol to CO_2 as compared with the commercial Pt black.

(63) Tacconi, N. R.; Lezna, R. O.; Beden, B.; Lamy, C. *J. Electroanal. Chem.* **1994**, *379*, 329–337.
(64) Hu, J. T.; Odom, T. W.; Lieber, C. M. *Acc. Chem. Res.* **1999**, *32*, 435–445.

Conclusions

For the first time, we have made use of Rh nanocubes as seeds to produce high-yield, high-selectivity Rh/Pt bimetallic ultrathin nanowires with nodes and stems structure via seed displacemnt, epitaxial growth method in a single aqueous phase. The electrocatalytic activity of these Rh/Pt ultrathin nanowires toward ethanol oxidation was investigated compared with the activity of the Rh nanocubes and the commercial Pt black. Thanks to the effective ability of Rh for breaking the strong C−C bond of ethanol and consecutive structure of ultrathin nanowires, the maximum selectivity to CO_2 of Rh/Pt nanowires is at least 2.69 times higher than that of commercial Pt black. The peak current is 1.2 times that of commercial Pt black and the potential decreased about 40 mV. This study displays a great significance in synthesis of high selectivity and activity catalysts for ethanol oxidation to CO_2, and in improvement of the efficiency of direct ethanol fuel cells as well.

Acknowledgment. This work was supported by NSFC (20725102, 20933004 and 20921001), the Fok Ying Tung Education Foundation (111012), and the State Key Project of Fundamental Research for Nanoscience and Nanotechnology (2006CB932301).

Supporting Information Available: TEM and STEM images, EDS profiles, elemental analysis results (PDF). This material is available free of charge via the Internet at http://pubs.acs.org.